Impact of Fuzz Button Degradation on AM and PRBS Signal Transmission

IET Microwaves, Antennas & Propagation

WILEY

The Institution of Engineering and Technology

ORIGINAL RESEARCH OPEN ACCESS

Impact of Fuzz Button Degradation on AM and PRBS Signal Transmission

Wenjia Wang[1,2] | Jinchun Gao[1] | Paolo Manfredi[2] | Igor S. Stievano[2]

[1]Beijing Key Laboratory of Work Safety Intelligent Monitoring, Beijing University of Posts and Telecommunications, Beijing, China | [2]Department of Electronics and Telecommunications, Politecnico di Torino, Turin, Italy

Correspondence: Jinchun Gao (gjc@bupt.edu.cn)

Received: 23 November 2024 | **Revised:** 18 March 2025 | **Accepted:** 10 April 2025

Handling Editor: Tim Brown

Funding: This work was supported in part by the National Key R&D Program of China (Grant No. 2022YFF0605904), in part by the Specialized Scientific Research Projects of Chinese Institute of Electronics and Beijing Smart-chip Microelectronics Technology Co. Ltd. in part by the BUPT Excellent Ph.D. Students Foundation under Grant No. CX2023201 and in part by Program of China Scholarship Council (Grant No. 202306470071).

Keywords: analog modulation (AM) signal | degradation mechanism | electrical contacts | electromagnetic compatibility | electromagnetic wave transmission | equivalent circuits | fuzz button connector | integrated circuit interconnections | pseudo random binary sequence (PRBS) signal | signal transmission

ABSTRACT

As elastic electrical connectors, fuzz buttons provide a vertical and solderless electrical interconnection in microwave modules to enhance the integration. However, prolonged use in harsh environments poses a risk of potential failure in electronic components, potentially compromising communication system reliability. This work studies the impact of fuzz button degradation in harsh environments on analog modulation (AM) and pseudo random binary sequence (PRBS) signal transmission using theoretical analysis and experimental testing. Accelerated tests are designed to obtain the fuzz button samples with different degradation levels. The surface morphology observation and elemental analysis are conducted to analyse the degradation mechanism. In addition, a transmission channel with fuzz button interconnections is designed and the corresponding equivalent circuit model is developed. Based on the proposed circuit model, the effects of fuzz button degradation on the integrity of both AM signal and PRBS signal are investigated by analysing the metrics such as waveform, eye diagram and bit error rate (BER) of the output signal. In addition, the effects of the carrier frequency of AM signals, and the transmission rate of the PRBS signals on signal transmission are also investigated. The simulation results of the circuit model show good agreements with experimental tests. The research results provide a better understanding regarding the potentially corrosive effects of harsh environments on fuzz button connectors and the negative effects on the signal integrity. Moreover, the research results provide comprehensive data support for identifying key features that are used for the development of machine learning models for fault diagnosis and localisation in radio frequency (RF) circuits with fuzz button interconnections.

1 | Introduction

Fuzz button connectors have become integral components in industries requiring reliable separable three-dimensional interconnections such as aerospace, electronics and automotive fields. They provide a vertical and solderless electrical interconnection solution that enhances the integration of complex electronic systems. Despite the growing application of fuzz buttons, existing studies primarily focus on their application and electrical/mechanical properties under standard operational conditions. For instance, Su et al. [1] proposed a 3D multi-channel amplifier module with fuzz buttons based on LTCC technology,

where fuzz buttons are used as input and output ports to transmit RF signals. Lu et al. [2] used fuzz buttons to make elastic connection with low temperature co-fired ceramic (LTCC) substrate and mother board to transmit power, control signals and RF signals in the design of a frequency synthesiser based on system in package (SIP) technology. Mechanical force was utilised to establish and maintain connections involving the fuzz buttons. For example, in the press-pack SiC MOSFET packaging, a clamping block was used to apply symmetrically distributed pressure, ensuring stable electrical contact between the fuzz buttons and the connected modules [3]. Similarly, in a four-channel T/R module design, alignment pin structures were incorporated at the corners of both the LTCC substrates and the fuzz button interposers, and mechanical pressure was applied to stack the submodules tightly [4]. Hauhe and Wooldridge [5] used the three-wire fuzz button in the design of X-band active array radars because of its very little voltage drop and excellent ground connection when compressed, making it well-suited for airborne environments where vibration does not induce modulation on the microwave carrier. Pan et al. [6] applied a quasi-static approach to find the distributed capacitance and inductance of the fuzz buttons. Furthermore, he established an equivalent non-uniform transmission line model for the fuzz button and conducted waveform simulation. Carter [7] proposed an equivalent circuit model of fuzz buttons, composed of resistance, capacitance and inductance, which is applicable across the frequency range from DC to 3.05 GHz. Harris and Pecht [8] studied the relationship between load, displacement and contact resistance using fuzz buttons with different materials, diameters and filling densities that provided technical support for the assembly and manufacture of electronic modules. Based on instantaneous estimation of wear rate, Lall et al. [9] proposed a wear simulation model for fretting of reciprocating curved spring-loaded contacts.

However, when subjected to prolonged operation in harsh environments, fuzz buttons will experience degradation due to environmental stresses such as temperature fluctuations, atmospheric corrosion and mechanical wear which could affect the reliability and performance. Previous studies on environmental impacts are limited in scope. For example, Wang, Gao, Flowers et al. [10] showed that long-time compression on fuzz buttons leads to an increase in resistance because of stress relaxation, but had little effect on high frequency transmission performance. Guarin and Longenbach [11] found that the contact resistance of fuzz-button based z-axis socket assemblies significantly increased after mating/un-mating cycles during high temperature operation, caused by the formation of an oxide layer on the substrate pad metallurgy. Almquist [12] showed that fuzz buttons had sufficiently low resistance to meet signal and power requirements in liquid nitrogen environment while also demonstrating that the resistance did not increase in high temperature/humidity environments. In addition, electronic materials are susceptible to corrosion when used in harsh environments for a long time, particularly in environments that contain moisture, dust and atmosphere pollutants, which brings significant challenges to safety and reliability. For example, Xiao et al. [13] investigated the corrosion mechanism of gold-plated printed circuit boards (PCBs) in atmospheric environment with high salinity, which revealed that microporous corrosion was the primary form of degradation affecting PCBs and the corrosion products consisted of oxides, chlorides, sulphates and carbonates of copper and nickel. Zhang [14] summarised the mechanism and characteristics of mobile phone connector contacts failure because of particle contamination. Based on multi-conductor transmission line theory and electrical properties of dendrite-like electrochemical migrated silver, Wang et al. [15] developed a distributed parameter circuit model for the circuit board with silver migration to analyse the high frequency behaviour.

The broader impact of environmental stress on signal transmission and the associated degradation mechanisms in fuzz buttons remain insufficiently addressed. Previous research analysed the effect of long-time compression and corrosive degradation of fuzz button on S-parameters from frequency domain perspective [10, 16]. Based on the previous findings, the current work further investigates the impact of fuzz button degradation on amplitude modulation (AM) and pseudo random binary sequence (PRBS) signal transmission from the time domain perspective. Fuzz buttons with different degradation levels were produced by accelerated tests, and the degradation mechanism was analysed by morphological observation and elemental analysis using a scanning electron microscope (SEM). Additionally, a transmission channel with fuzz button interconnections before and after degradation was designed and the corresponding parasitic electrical parameters of the impedance network in the model were extracted. Based on the proposed circuit model, the key metrics of the output signal such as modulation index, sideband and carrier components were analysed when the excitation source was AM signal. The output waveforms, eye diagrams and bit error rate (BER) were also analysed when the excitation source was the PRBS signal. The simulation results are consistent with the experimental test results. The current work is an extension and further refinement of the previous study, expanding the scope of the investigation. The multi-perspective analysis across the time and frequency domains provides more comprehensive data support for subsequent research of fault diagnosis and localisation [17, 18]. By analysing the impact of fuzz button degradation on waveforms, eye diagrams ands BER, combined with S-parameters from previous studies, the key features can be selected from both time and frequency domains which is useful for developing the machine learning models for automated fault diagnosis and localisation of fuzz button interconnections in radio frequency (RF) circuits.

2 | Experimental Testing

Degradation mechanisms of fuzz buttons under harsh environments are essential for evaluating the degradation behaviours of fuzz buttons. Accordingly, accelerated tests were conducted using corrosive gas and nitric acid vapours to simulate the atmospheric corrosion. The following section describes the experimental setup and procedure of the accelerated tests as well as the discussion of the results.

2.1 | Experimental Setup

The fuzz buttons with a diameter of 0.5 mm and a height of 2.6 mm were selected as test samples. The diameter of the metal

wire was 0.045 mm and its gold plating thickness was 0.3 μm. The base material of the metal wires was copper-beryllium alloy, and the cladding materials were nickel and gold that aimed to improve electrical conductivity and oxidation resistance. The new fuzz button samples were exposed to the nitric acid vapour with 65%–68% concentration for 20, 35 and 45 min, respectively, and they were defined as degraded Level-1, degraded Level-2 and degraded Level-3 samples, respectively. The degraded samples were then dried in a drying oven at 150°C for 20 min and then at room temperature for 72 h. The surface morphology and composition analysis of the fuzz buttons before and after degradation were measured using a SEM. In addition, the thickness of the corrosion products was typically measured using a metallographic microscope.

As shown in Figure 1a, the device under test (DUT) was specifically designed to analyse the impact of fuzz button degradation in harsh environments on signal transmission. The DUT consists of sub miniature version A (SMA) connectors, two coplanar waveguide PCBs, a dielectric block and the fuzz button connectors before and after degradation. Two coplanar waveguide PCBs served as the transmission path for electromagnetic waves to simulate practical application scenarios. SMA connectors were welded in the PCBs to connect the transmission channel to the test equipment. The fuzz buttons were placed within the drilled holes of the dielectric block. As shown in Figure 2, the DUT featured a stacked structure with the test fixture providing the necessary mechanical force. The initial length of the fuzz buttons exceeded the height of the dielectric block. When the test fixture applied a normal force, the fuzz buttons were compressed, aligning their height with that of the dielectric block. The fuzz buttons were elastically deformed, ensuring consistent contact with both the upper and lower PCBs, effectively realising stable electrical interconnections between the modules. The DC resistances of the samples were measured using a RIGOL DM3061 digital multimeter. The testing points were fixed to ensure that any differences in measured resistance values are due to differences in the fuzz buttons degradation. The high-frequency parameters of the transmission channel were measured using an Agilent N5230C vector network analyser (VNA) with the number of sampling points set at 201. The VNA was calibrated through a short/open/load/through (SOLT) procedure before each measurement to eliminate the impacts of cables on the experimental tests.

2.2 | Experimental Results

Figure 3 shows the SEM images of the fuzz button samples, and the main chemical composition of test locations in weight percentage (wt%) are summarised in Table 1. The elements include carbon (C), oxygen (O), gold (Au), nickel (Ni), and copper (Cu). The main elements of Spot1 are copper, nickel, and gold with 33.4%, 32.6% and 25.1% in weight, respectively. The main elements of Line1 are oxygen and copper with 18.7% and 52.9% in weight, respectively. The results indicate that exposure to corrosive environments leads to fuzz button degradation and the corrosion products mainly consist of copper oxides with trace amounts of unoxidised metals. The corrosive products are attached to the metal wire surfaces of the degraded fuzz buttons

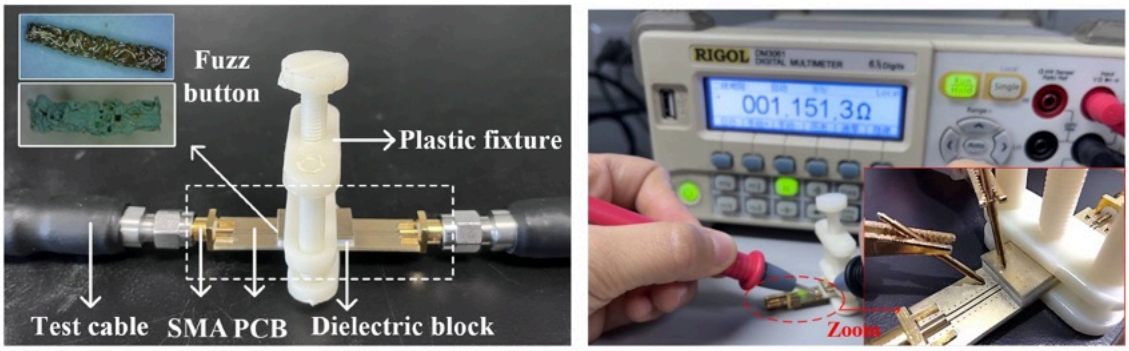

FIGURE 1 | Measurement setup. (a) High-frequency parameters measurement. (b) Contact resistance measurement.

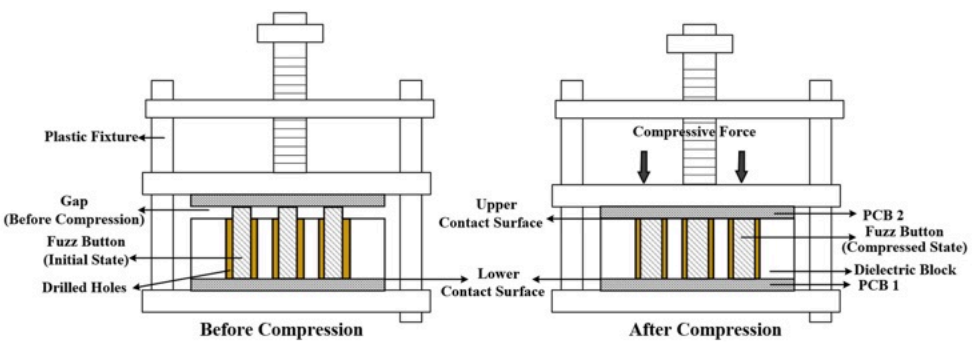

FIGURE 2 | Schematic diagram of compression process.

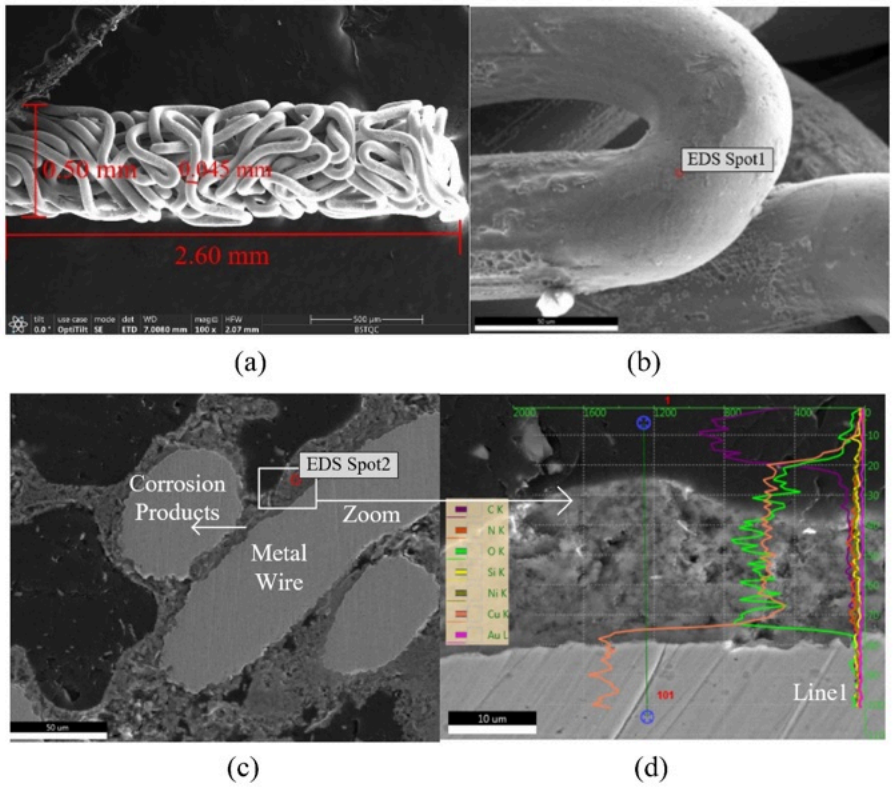

FIGURE 3 | SEM morphology of fuzz button samples. (a) SEM morphology of an undegraded sample. (b) Magnified SEM image of undegraded sample. (c) Cross-sectional morphology of degraded Level-3 sample. (d) Cross-sectional morphology of degraded Level-3 sample with element distributions along the green line.

TABLE 1 | Main chemical composition of test locations (wt%).

Elements	C	O	Au	Ni	Cu
Spot1	7.3	1.7	25.1	32.6	33.4
Line1	19.9	18.7	3	1.1	52.9

caused by microporous corrosion. When fuzz buttons are exposed to corrosive environments, the nickel and copper layers are in direct contact with the external environments through the micropores on the gold layer that serve as the active areas for the microporous corrosion. In this process, the corrosive gases act as the electrolyte, while gold functions as the cathode and nickel and copper act as the anodes. Over time, corrosion products accumulate within the micropores and gradually migrate from these pores to the surface of the metal wires. The amount of corrosion products increases as the exposure time increases. As a result, the pores are filled with corrosion products, forming mound-like clusters on the surface that eventually interconnect.

As shown in Figure 4, the actual distribution of corrosion products on the metal wires of the degraded fuzz button is non-uniform and complex because of uneven thickness of the gold layer. The corrosion products thicknesses at points 1–8 were measured to obtain the average thickness of the corrosion film. The average corrosion film thicknesses for degraded Level 1–3 are 12.02, 14.59 and 22.61 μm, respectively. The measurement results of the total resistance for degraded Levels 1-3 samples are 0.73, 1.28 and 3.33 Ω, respectively. The measured S parameters

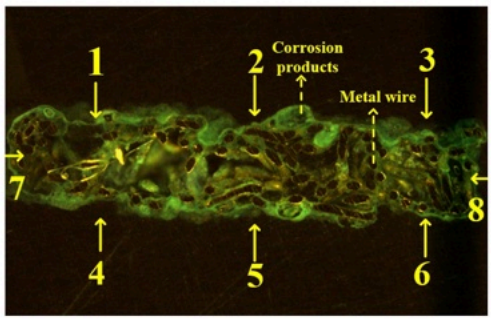

FIGURE 4 | Enlarged image of a cross-section of a degraded fuzz button.

for the transmission channel with the fuzz button before and after degradation are shown in Figure 5. For each degradation level, the experimental tests were repeated three times, and the results demonstrated good repeatability. The frequency range is from 10 MHz to 4 GHz. The S parameters values are related to frequency and degradation level. S_{11} values at high frequency are higher than those at low frequency, and S_{21} values at high frequency are lower than those at low frequency. Under a given point, most of the S_{11} values increase while S_{21} values decrease with the increase of degradation level, respectively. In addition, the reflected voltage and time domain reflectometry (TDR) results are obtained by post-processing the two-port S-parameter (S2P) data of the transmission channel obtained from the experimental tests. As shown in Figure 6, the impedance peaks in the TDR curve occur at 0.303 and 0.563 ns, corresponding to

the locations of two fuzz button transition areas. Fuzz button transition structure displays an inductive characteristic. Compared to the undegraded case, the impedance discontinuity increases when the fuzz buttons degrade with a clear difference between the curves starting from the first peak P. This is because the accumulation of corrosion products and thickening of corrosion film alter the electrical parameters in the impedance network of the fuzz button interconnection. Compared to the undegraded ones, the reflected voltage values of the transmission channel with degraded Level-3 fuzz buttons increase by 0.057, 0.145 and 0.075 V in peak M, N and final voltage, respectively, indicating fuzz button degradation aggravates electromagnetic waves reflection. The curves in Figure 6a,b exhibit similar trends over time, with variations only in the vertical axis parameters.

3 | Model Development

To better understand the effect of fuzz button degradation on signal transmission, the equivalent circuit model is developed for the DUT with fuzz buttons before and after degradation as shown in Figure 7a. The material of the signal and ground conductors of the PCBs is copper. The dielectric layer of PCB is FR4 and its thickness is 0.61 mm. The dielectric block provides both alignment feature and physical protection for the fuzz buttons. The length and width of the dielectric block are the same as the PCB2. The material name of the dielectric block is Alumina Ceramics with a relative dielectric constant of 9.28 and a loss tangent of 5.4×10^{-3} (at 1 GHz). The fuzz buttons in the transition area serve as vertical electrical interconnects between the PCBs, designed as a three transmission-line (GSG) structure to enhance signal transmission reliability and stability. As shown in Figure 7a, in the equivalent circuit model, the SMA, PCB 1 and PCB 2 parts are simulated using the electromagnetic field simulation software, and the corresponding S2P files are extracted.

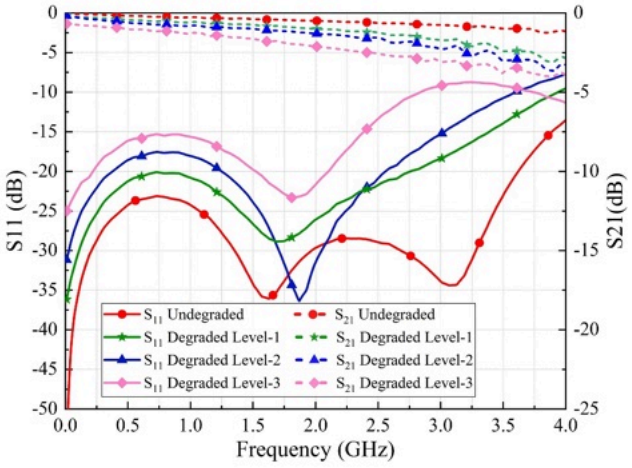

FIGURE 5 | S parameters of transmission channel obtained from experimental measurements.

For the undegraded fuzz button interconnection with GSG structure, it is modelled as π impedance network composed of equivalent inductance and equivalent capacitance as described by Wang, Gao, Flowers et al. [10]. For the degraded fuzz button interconnection, corrosive products attach on the metal wires within degraded samples because of the porous structure, leading to a majority of contact points being in metal-corrosion film-metal contact states. When the signal flows through the degraded contact points, the corrosion spots have an inductive effect at high frequency band, and the conductivity of the corrosion spots is low, resulting in an increase in the contact inductance L_{cf} and bulk resistance R_{bulk} of the degraded samples. Because of corrosion effects, the reduction in the height of the fuzz button conductor also leads to a reduction in the self-inductance $L_{sf.}$ As shown in Figure 8, the contact surface between the fuzz button and the copper plate is not perfectly smooth on the microscopic scale, and only contacts at some convex discrete spots on the two rough surfaces. The current flow path narrows as it passes through the discrete points, which causes the currents to bunch together and creates constriction resistance. In areas where no contact occurs, high-frequency current passes through the contact interface via capacitive coupling, resulting in contact capacitance. When corrosion products cover some areas of the contact surface, the equivalent resistivity and the equivalent dielectric constant of the contact interface change, affecting contact resistance and the contact capacitance [19]. Based on the electrical contact theory, a degraded contact surface can be modelled as a parallel network of contact resistance R_{cf} and contact capacitance C_{cf}. The contact impedance and contact capacitance can be expressed as follows:

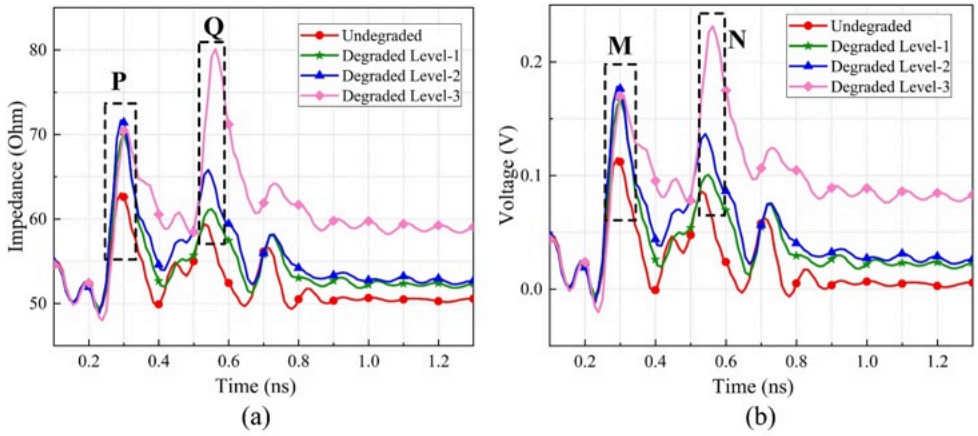

FIGURE 6 | TDR results and reflected voltage for different degradation levels. (a) TDR results. (b) Reflected voltage.

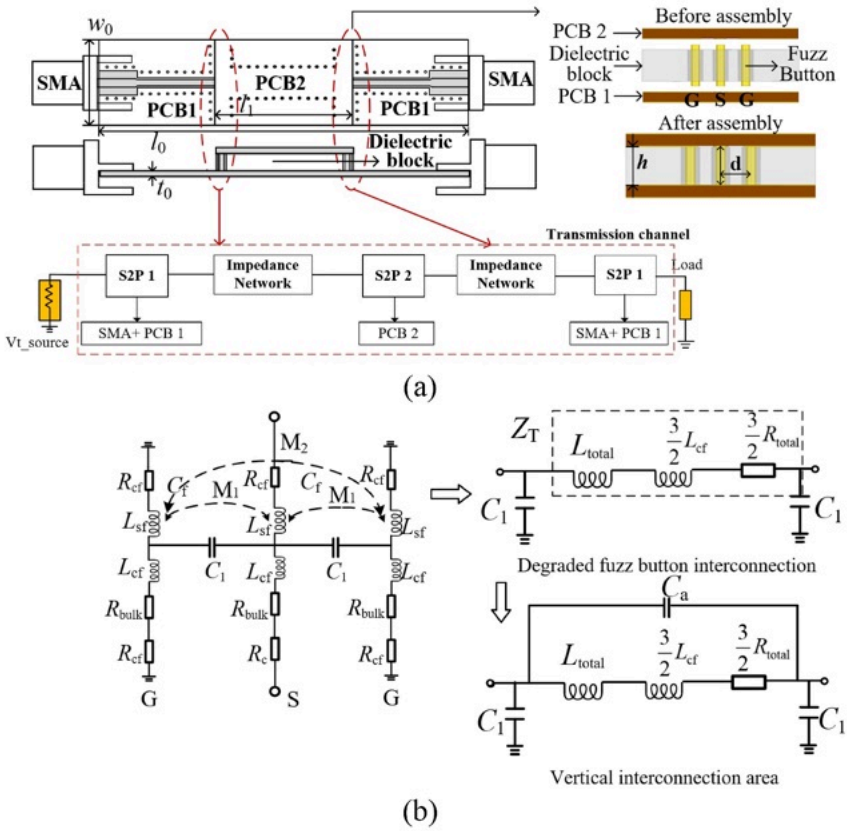

FIGURE 7 | Schematic diagram and parasitic electrical parameters of transmission channel. (a) Transmission channel with fuzz button interconnections. (Dielectric block height h = 2.0 mm, distance between signal conductor and ground conductor d = 1.6 mm, l_0 = 43.2 mm, w_0 = 10 mm, l_1 = 16.1 mm and t_0 = 0.702 mm). (b) Impedance network of the fuzz button interconnection.

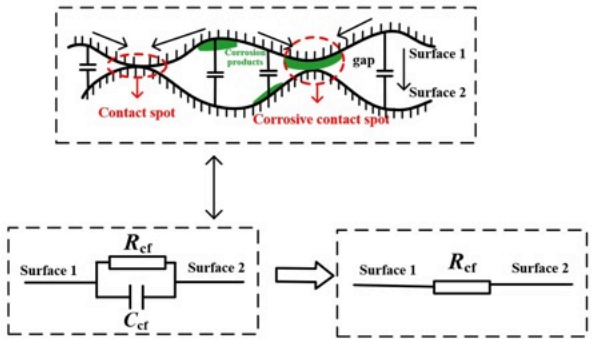

FIGURE 8 | Interface between two rough surfaces in contact.

$$Z_c = \frac{R_{cf}}{1 + j\omega C_{cf} R_{cf}} \tag{1}$$

$$C_{cf} = \frac{\varepsilon_0 \varepsilon_f \pi {r_0}^2}{H_{cf}} \tag{2}$$

where $\omega = 2\pi f$, f is signal frequency. ε_f is the relative dielectric constant of the corrosion film. H_{cf} is corrosion film thickness. For different degradation levels samples, the values of $\omega C_{cf} R_{cf}$ at 4 GHz are $0.045R_{cf}$, $0.037R_{cf}$ and $0.024R_{cf}$, respectively. As noted above, the overall resistance values ($2R_{cf}$ + R_{bulk}) of the degraded level 1-3 samples are 0.73, 1.28 and 3.33 Ω, respectively. Accordingly, the values of $\omega C_{cf} R_{cf}$ are much less than 1, and Z_c can be approximated by R_{cf}. The parasitic parameters of a degraded fuzz button are shown in Figure 7b which is modelled as contact resistance R_{cf}, self-inductance L_{sf}, contact inductance L_{cf} and bulk resistance R_{bulk} in series. C_1 is the equivalent capacitance between the signal fuzz button and the ground fuzz button. As shown in Figure 9a, when fuzz buttons degraded, the corrosion products attached on the surface of the sample, altering the dielectric material between the signal fuzz button and ground fuzz button from an air gap-dielectric block configuration to a corrosion film-air gap-dielectric block configuration. To facilitate research, the complex and non-uniform distributed corrosion products on the fuzz button surface are simplified to a uniform corrosion film.

The equivalent impedance network for the fuzz button interconnection is as follows:

$$\begin{aligned} Z_T &= \left(2R_{cf} + j\omega(L_{sf} - M_1) + j\omega L_{cf} + R_{bulk}\right) \\ &\quad + \frac{1}{2}\left(2R_{cf} + j\omega(L_{sf} - 2M_1 + M_2) + j\omega L_{cf} + R_{bulk}\right) \\ &= j\omega\left(\frac{3}{2}L_{sf} - 2M_1 + \frac{1}{2}M_2 + \frac{3}{2}L_{cf}\right) + \frac{3}{2}R_{total} \\ &= j\omega\left(L_{total} + \frac{3}{2}L_{cf}\right) + \frac{3}{2}R_{total} \end{aligned} \tag{3}$$

where the resistance values R_{total} are measured by RIGOL DM3061 digital multimeter. The equivalent contact inductance L_{cf} is extracted by fitting the simulation results with the

experimental results and the values for different degradation levels are 0.4, 0.45 and 0.53 nH, respectively. L_{total} is the equivalent inductance of the fuzz buttons interconnection. L_{sf} is the self-inductance of degraded samples. M_1 and M_2 are mutual inductances between the signal fuzz button and ground fuzz button, and between the ground fuzz button, respectively. The inductance values and the equivalent capacitance between the signal fuzz button and the ground fuzz button C_1 were obtained by electromagnetic field model simulation. The voltage of the signal conductor is set as 1 V, and the voltages of the two ground conductors are set as 0 V. As mentioned before, the main corrosion products are copper oxides. The relative dielectric constant of copper(II) oxide (CuO) aries between 25 and 10^3, whereas that of copper(I) oxide (Cu_2O) is about 7 [20]. The relationship between equivalent capacitance and relative dielectric constant of the corrosion products is shown in Figure 9b. Increases in both degradation level and relative dielectric constant result in an increase in equivalent capacitance. However, compared to the effect of degradation level on capacitance, changes in relative dielectric constant have a very small effect on the equivalent capacitance. The equivalent capacitances for the three degradation levels are set as 0.0625, 0.0635 and 0.0660 pF, respectively. In addition, the parasitic capacitance C_a in the top and bottom transition area is considered, which is similar to a plate capacitance, which can be calculated by the following equation:

$$C_a = \frac{\varepsilon_0 \varepsilon_p A}{h} \tag{4}$$

where A and h are the overlap area and the separation distance of the top and bottom transition surfaces, respectively.

ε_p is the relative dielectric constant of the dielectric block. The value of parasitic capacitance is 0.15 pF. The impedance network of the vertical structure for the transmission channel is shown in Figure 7b and the corresponding parasitic electrical parameters are shown in Table 2.

4 | Results and Discussion

AM signal and PRBS signal are employed to evaluate the impact of fuzz button degradation on signal transmission from the time-domain perspective. Since the AM signal is highly sensitive to changes in the integrity of the transmission path, it can be used as an effective indicator to evaluate the overall performance, thereby indirectly reflecting the degradation of key components such as the fuzz button. Meanwhile, the PRBS signal, widely used for assessing the communication quality of high-speed digital transmission systems, is particularly effective in detecting signal integrity issues caused by component degradation. By comparing the key electrical metrics before and after degradation, this section provides a comprehensive evaluation of signal quality deterioration caused by fuzz button degradation and identifies potential failure modes in RF circuits. The following analysis presents detailed results and discussions.

4.1 | AM Signal Transmission

The block diagram of the amplitude modulation is illustrated in Figure 10a. The baseband modulation signal is $m(t) = m_\alpha A_0 \sin(2\pi f_m t)$,

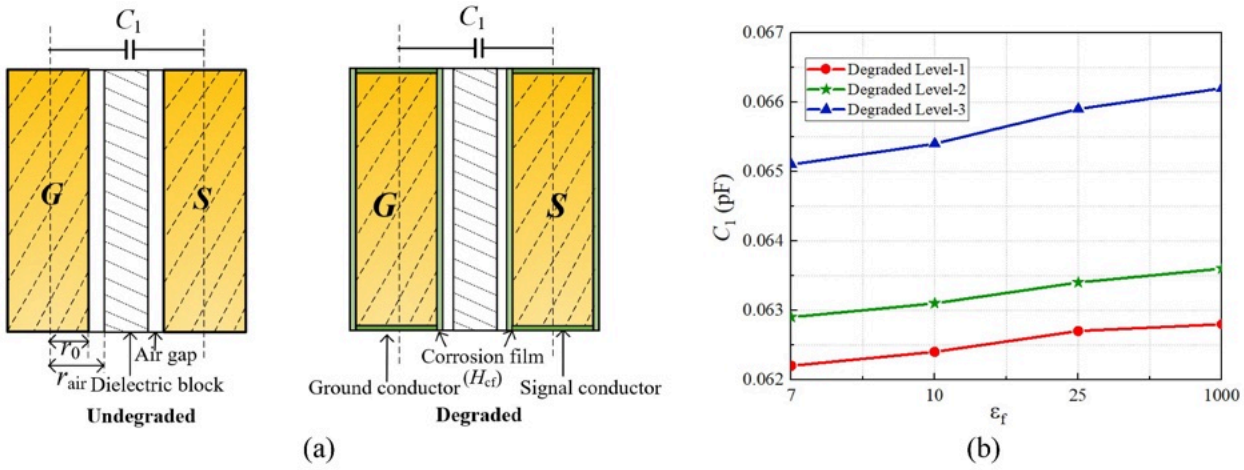

FIGURE 9 | Analysis of equivalent capacitance of the degraded fuzz button interconnection. (a) Schematic diagram of the equivalent capacitance between signal fuzz button and ground fuzz button (fuzz button radius in compression states r_0 = 0.28 mm and radius of drilled hole r_{air} = 0.5 mm). (b) Relationship between the equivalent capacitance C_1 and the relative dielectric constant of corrosive products.

TABLE 2 | Parasitic electrical parameters of fuzz button interconnection.

	H_{cf} (μm)	R_{total} (Ω)	L_{sf} (nH)	M_1 (nH)	M_2 (nH)	L_{total} (nH)	C_1 (pF)	L_{cf} (nH)
Undegraded	—	0.02	0.727	0.228	0.125	0.697	0.060	—
Degraded Level-1	12.02	0.73	0.714	0.224	0.122	0.684	0.0625	0.40
Degraded Level-2	14.59	1.28	0.711	0.223	0.122	0.682	0.0635	0.45
Degraded Level-3	22.61	3.33	0.703	0.220	0.120	0.675	0.0660	0.53

where $m_a = 0.1$ is the modulation index, and $f_m = 10$ MHz is the frequency of the baseband modulation signal. The carrier signal is $c(t) = A_0\cos(2\pi f_c t)$, where f_c MHz is the frequency of the carrier signal and t is time. A_0 is the amplitude of the carrier signal with a value of 1 V. The transmission channel is the equivalent circuit shown in Figure 7. V_{out} is output signal. R_{L1} is circuit load. The AM signal $V_{\text{AM}}(t)$ in the time domain is as follows:

$$V_{\text{AM}}(t) = [A_0 + m(t)]\cos(2\pi f_c t) \tag{5}$$

The output waveforms of the AM signal transmitted through the channel with undegraded and degraded Level-3 fuzz button interconnections are illustrated in Figure 11, respectively, when f_c is 100 MHz. A_m represents the sideband component amplitude and U_c represents the carrier component amplitude. The modulation index, m_{a1}, is defined as the ratio of A_m to U_c. For all degraded output waveforms, the modulation index remains approximately 0.1, consistent with that of the undegraded signals. This indicates that the fuzz button degradation does not change the modulation characteristics. Furthermore, compared

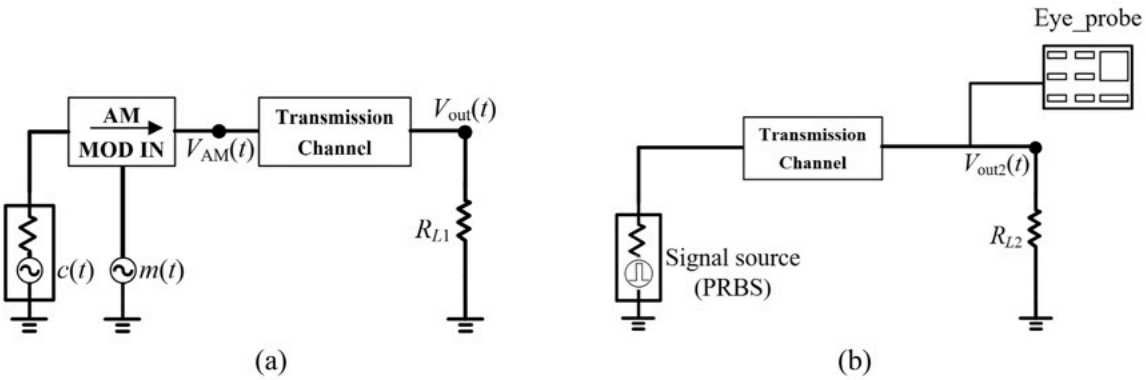

FIGURE 10 | Block diagram. (a) AM signal transmission. (b) PRBS signal transmission.

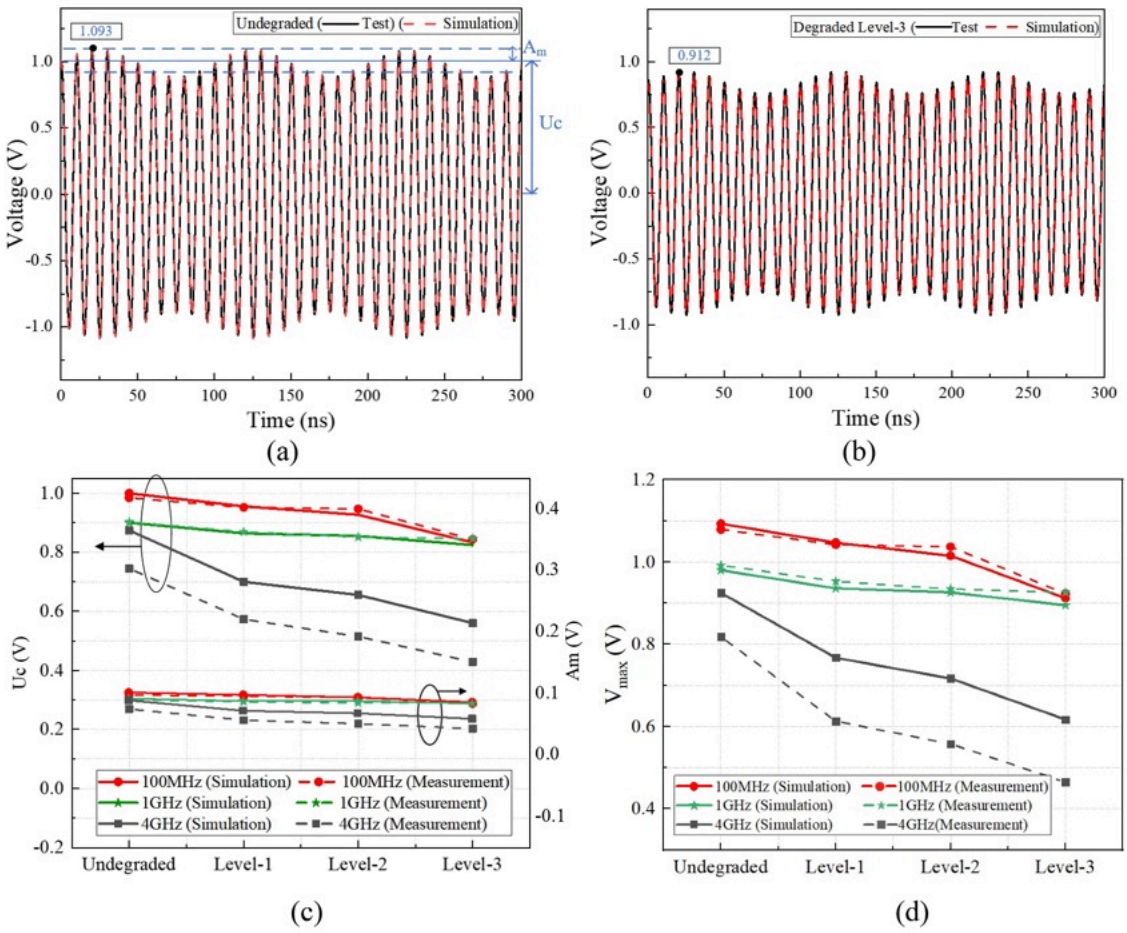

FIGURE 11 | Waveform analysis of output signal. (a) Output waveforms for undegraded case (f_c = 100MHz). (b) Output waveforms for degraded Level-3 case (f_c = 100MHz). (c) Amplitudes of carrier component and sideband component. (d) Maximum amplitude of output waveforms.

to the undegraded ones, the carrier frequency of the degraded output waveforms remains stable with no frequency shift. Inspection of Figure 11a,b reveals that the shapes of the output waveforms remain similar but the amplitudes are different. To further quantify the impact of degradation, the values of U_c and A_m for output waveforms under different degradation levels and frequencies are analysed and presented in Figure 11c. The results demonstrate that, for a given degradation level, the amplitudes of both the carrier component and the sideband component decrease as the frequency increases. Consequently, the maximum amplitudes of the output waveforms also exhibit a decreasing trend. This is mainly because the wavelength of an electromagnetic wave is long and the effect of transmission channel structural discontinuity on signal transmission is small when the carrier signal frequency is low. The wavelengths of the electromagnetic waves become increasingly shorter with the increase of frequency, and therefore any small change of transmission channel may result in an obvious effect on the electromagnetic wave reflection, leading to a higher amplitude attenuation. In addition, for a given frequency, the amplitudes of the carrier component and the sideband component decrease with the increase of degradation level. Because the structures of the PCB 1 and PCB 2 remain unchanged in all simulations and measurements, the differences in waveform amplitudes are mainly due to vertical interconnection variations caused by the degradation of fuzz buttons. As shown in Figures 5 and 6, fuzz button degradation results in more severe impedance mismatch, more electromagnetic wave reflection, and greater transmission loss. Consequently, for a given carrier frequency, the amplitude of the output waveforms decreases with the increase of degradation level. The comparisons between the output waveforms obtained from the equivalent circuit model and experimental tests show overall good agreements. The experimental values are slightly smaller than the simulation results in the high frequency band which is mainly because of circuit model simplification, the minor variations between the model and actual physical samples and measurement error.

4.2 | Digital Signal Transmission

The block diagram is illustrated in Figure 10b. The single-polarity PRBS signal with 13-order is selected as the excitation signal. The rise time of the PRBS signal is set to 48 ps and the transmission rate is 4 Gbps. The high voltage level is set to 1 V and the low voltage level is set to 0 V. The transmission channel is the equivalent circuit shown in Figure 7. R_{L2} is circuit load. V_{out2} is the output signal.

To illustrate the effect of fuzz button degradation in the transmission channel on high-speed digital signal transmission, the cases of undegraded and degraded Level-3 are analysed as examples. The output waveforms of signals passing through the transmission channel for the cases of undegraded and degraded Level-3 are shown in Figure 12a,b. A comparison of the results obtained from the equivalent circuit model and experimental tests shows good agreements, confirming the validity of the proposed model. The amplitudes of output waveform for the transmission channels decrease with the increase of degradation level. The output waveform amplitudes of the transmission channel with Degraded Level 1-3 samples are 0.973, 0.949 and 0.850 V, respectively, which are lower by 0.024, 0.048 and 0.147 V than the value for undegraded voltage. This is because the waveform amplitude is mainly determined by low-frequency components of the signal, whereas the rising/falling edge is mainly determined by high-frequency components. As indicated in Table 2, both the resistance and the sum of inductance in the equivalent impedance network of the fuzz button interconnections increase as the degradation level increases, and therefore the low-frequency component loss of the signal increases as it transmits through the channel, leading to a decline in output waveform amplitude. In addition, there is approximately 372.3 ps delay between the output signals and the original input PRBS signal, attributed to the propagation time of electromagnetic wave in the transmission channel.

Eye diagram is an important characteristic to evaluate transmission channel quality. The eye diagrams corresponding to the undegraded and degraded Level-3 cases are presented in Figure 12c,d. The eye diagram of the undegraded channel is of good quality as evidenced by the smoothness of Level 0 and Level 1, and the good overlap of the rising edges and the falling edges. The eye diagram deteriorates as the degradation level increases, reflecting in the smaller eye opening, greater average rise time, noise amplitude and peak-to-peak jitter (jitter PP). Specifically, compared to undegraded case, the corresponding height and width of the eye diagram for the degraded Level-3 case decrease by 0.172 V and 7 ps, respectively. Additionally, the eye diagram data for other degradation levels are summarised in Table 3. The eye diagrams from experimental measurements have the same trends as those from the circuit models.

Bit error rate (BER) is another pivotal parameter in communication. The BER values for the undegraded and degraded Level-3 cases are investigated through timing bathtub and voltage bathtub as shown in Figure 12e,f. For the undegraded case, the timing bathtub curve shows a wide flat region where BER remains below 1×10^{-16} which suggests the system can tolerate substantial sampling timing variations without a significant rise in BER. For the degraded Level-3 case such a flat region narrows slightly. The voltage bathtub curve for the undegraded case shows a wide flat region (0.03–0.95 V) with BER consistently maintained below 1×10^{-16}, demonstrating a high noise margin. However, for the degraded Level-3 case, the BER rises significantly at low-voltage (from 0.03 to 0.07V) and high-voltages (from 0.95 to 0.78 V) regions. It is clear that the degradation of the fuzz buttons leads to an increase in the BER of the output signal that can be explained by the observed rise in the average rise time and jitter PP with increasing degradation. The increase in rise time leads to inter-symbol interference (ISI) primarily. In high-speed communication systems, where the symbol width is short, an increase in rise time results in current symbol interfering with the sampling point of the subsequent symbol. This reduces the signal's discernibility and increases the BER. In addition, a greater jitter affects the accurate location of eye crossing, leading to misjudgement and misinterpretation of signals.

Eye diagram parameters corresponding to different transmission rates of the PRBS signal are also summarised in Table 3. The results indicate that for the same degradation level, the eye-opening decreases significantly and jitter PP increases as the

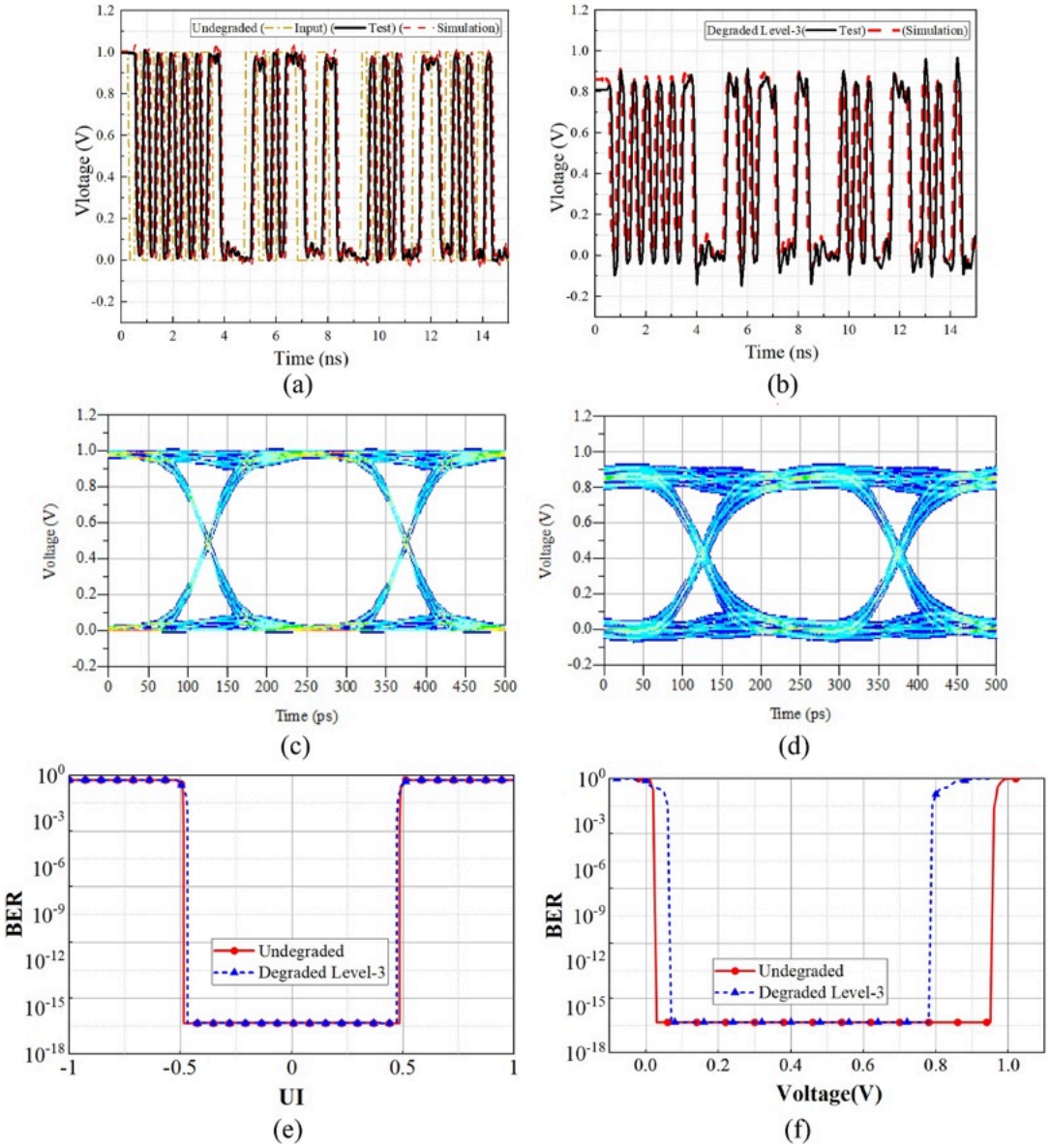

FIGURE 12 | Analysis of the effect of fuzz button degradation on 4 Gbps PRBS signal transmission from waveforms, eye diagram and BER. (a) Output waveforms for the undegraded case. (b) Output waveforms for the degraded Level-3 case. (c) Eye diagram for the undegraded case. (d) Eye diagram for the degraded Level-3 case. (e) Timing BER bathtub curves of the undegraded case and degraded Level-3 case. (UI is Unit Interval). (f) Voltage BER bathtub curves of the undegraded case and degraded Level-3 case.

data rate increases. Additionally, under higher degradation levels and faster data rates, the rise time of the output signal increases significantly. For instance, when an 8 Gbps PRBS signal is transmitted through a transmission channel with degraded Level-3 fuzz buttons, the rise time obtained from experimental tests increases to 71.78 ps which is 23.78 ps longer than that of the input signal. The degradation in rise time can be attributed to severe high-frequency attenuation in the transmission channel that is clearly reflected in the S_{21} parameter. Figure 5 illustrates that S_{21} decreases as frequency increases, indicating greater attenuation at higher frequencies. In addition, S_{21} in the high frequency band becomes more significantly lower as the degradation level increases. Because of the wider main lobe of high-speed transmission rate (e.g., 8 Gbps) PRBS signals, greater signal loss occurs when passing through the transmission channel because of high-frequency attenuation. This high-frequency attenuation slows down the signal edges, leading to an increase in the rise time of the output signal. In the current work, for the transmission channel with undegraded and low degradation levels, the S_{21} value varies less between high and low frequencies, indicating that the high and low frequency components are attenuated to a similar degree. Consequently, although the main lobe of an 8 Gbps PRBS signal is wider than that of a 1 Gbps PRBS signal, the rise time of the two do not show a significant difference. However, as the degradation level increases (e.g., degradation Level-3), S_{21} in the high frequency band declines significantly compared to the low frequency band. As a result, under such conditions, compared to the PRBS signal with 1 Gbps, the rise time of the signal with 8 Gbps shows a significant increasing trend. The combined analysis of increased jitter, reduced eye opening and increased rise time at higher data rates highlights the challenges of

TABLE 3 | Specific corresponding parameters for the eye diagram.

		Simulation				Measurement			
	Rate (Gbps)	Eye height (V)	Eye width (ps)	Jitter PP (ps)	Rise time (ps)	Eye height (V)	Eye width (ps)	Jitter PP (ps)	Rise time (ps)
Undegraded	1	0.991	998	2.4	52.67	0.981	998	2.4	54.73
	4	0.952	238.5	11	53.94	0.912	244.0	6.5	53.26
	8	0.88	107.95	18.4	51.58	0.73	107.55	17.55	51.84
Degraded Level-1	1	0.939	998	2.8	56.31	0.93	998	3.6	55.83
	4	0.887	236.5	13	61.14	0.876	242.7	7.8	57.27
	8	0.67	89.3	19.8	55.97	0.56	94.55	19.95	59.41
Degraded Level-2	1	0.916	1000	1.6	55.84	0.906	997	3.2	56.89
	4	0.861	236	13.5	61.87	0.822	241.2	9.3	59.14
	8	0.62	87.35	23.4	57.52	0.51	91.65	24	61.35
Degraded Level-3	1	0.805	998	2.0	57.93	0.846	998	3.2	60.25
	4	0.765	235.5	14.5	64.93	0.740	237	13	63.63
	8	0.50	87.8	18	62.61	0.35	97	20.05	71.78

maintaining signal integrity in degraded channels, especially for high-speed communication systems.

5 | Summary and Conclusion

This work demonstrated the mechanism of fuzz button degradation in harsh environments and the effect of degradation on AM and PRBS signal transmission from a combined time and frequency domain perspective. Exposure to a corrosive environment led to microporous corrosion in fuzz buttons and the corrosion products mainly consisted of copper oxides with trace amounts of unoxidised metals. A transmission channel with fuzz button interconnections before and after degradation and the corresponding equivalent circuit model were proposed. Fuzz button degradation altered the parasitic electrical parameters of the equivalent circuit, affecting the impedance matching performance and the signal integrity of the transmission channel. Both simulation and experimental results consistently demonstrated that fuzz button degradation led to the signal integrity deterioration which is reflected in waveform distortion, smaller eye opening and increased BER of the output signal. The results of this investigation provide a better understanding of the influence of fuzz button degradation on signal transmission and validate modelling and analysis tools to evaluate such effects. Additionally, based on the waveforms, eye diagrams and BER from the current work, combined with S-parameters, the multi-angle analysis across time and frequency domains provides more comprehensive data support for identifying key features. These key features enable the development of machine learning models for fault diagnosis and localisation in RF circuits with fuzz button interconnections.

Author Contributions

Wenjia Wang: data curation, investigation, methodology, validation, writing – original draft, writing – review and editing. **Jinchun Gao:** investigation, resources. **Paolo Manfredi:** writing – original draft, writing – review and editing. **Igor S. Stievano:** writing – original draft, writing – review and editing.

Acknowledgements

This work was supported in part by the National Key R&D Program of China (Grant No. 2022YFF0605904), in part by the Specialized Scientific Research Projects of Chinese Institute of Electronics and Beijing Smartchip Microelectronics Technology Co. Ltd. in part by the BUPT Excellent Ph.D. Students Foundation under Grant No. CX2023201 and in part by Program of China Scholarship Council (Grant No. 202306470071).

Conflicts of Interest

The authors declare no conflicts of interest.

Data Availability Statement

The data that support the findings of this study are available from the corresponding author upon reasonable request.

References

1. J. Su, B. Li, X. Yao, and F. Su, "A 3D Multi-Channel Amplifier Module With Fuzz Button in LTCC," in *2023 3rd International Conference on Electronic Information Engineering and Computer (EIECT)* (2023), 240–243, https://doi.org/10.1109/EIECT60552.2023.10442107.

2. J. Lu, L. Zhou, L. Duan, H. Liu, T. Yu, and J. Chang, "Research of Frequency Synthesizer Based on SIP Technology With Novel Structure," in *2020 International Conference on Microwave and Millimeter Wave Technology* (2020), 1–3, https://doi.org/10.1109/ICMMT49418.2020.9386978.

3. N. Zhu, H. A. Mantooth, D. Xu, M. Chen, and M. D. Glover, "A Solution to Press-Pack Packaging of SiC MOSFETS," *IEEE Transactions on Industrial Electronics* 64, no. 10 (October 2017): 8224–8234, https://doi.org/10.1109/TIE.2017.2686365.

4. E. Koç, N. Öznazlı, and F. Altuntaş, "High-Performance Miniaturized Quad T/R Module for X-Band Low-Profile AESA," in *2022 19th European Radar Conference (EuRAD)* (2022), 309–312, https://doi.org/10.23919/EuRAD54643.2022.9924974.

5. M. S. Hauhe and J. J. Wooldridge, "High Density Packaging of X-Band Active Array Modules," *IEEE Transactions on Components Packaging & Manufacturing Technology Part A Part B* 20, no. 3 (1997): 279–291, https://doi.org/10.1109/96.618228.

6. G. Pan, X. Zhu, and B. Gilbert, "A Quasi-Static Analysis of Fuzz Button Interconnects," in *Proceedings 1993 IEEE Multi-Chip Module Conference* (1993), 85–91, https://doi.org/10.1109/MCMC.1993.302146.

7. D. Carter, "'Fuzz Button' Interconnects at Microwave and Mm-Wave Frequencies," *IEE Seminar on Packaging and Interconnects at Microwave and mm-Wave Frequencies* 2000 (2000): 1–6, https://doi.org/10.1049/ic:20000419.

8. D. B. Harris and M. G. Pecht, "A Reliability Study of Fuzz Button Interconnects," *Circuit World* 21, no. 2 (1995): 12–18, https://doi.org/10.1016/0026-2714(96)84456-8.

9. P. Lall, D. Shinde, B. Rickett, and J. Suhling, "Finite Element Models for Simulation of Wear in Electrical Contacts," in *11th Intersociety Conference on Thermal and Thermomechanical Phenomena in Electronic Systems* (2008), 836–841, https://doi.org/10.1109/ITHERM.2008.4544353.

10. W. Wang, J. Gao, G. T. Flowers, Z. Wang, and L. Bi, "Investigation of Signal Integrity of Fuzz Button Connectors under Different Compression States," *Microwave and Optical Technology Letters* 65, no. 7 (2023): 1959–1967, https://doi.org/10.1002/mop.33665.

11. F. J. Guarin and K. F. Longenbach, "Contact Resistance Degradation in Z-axis Connectors Operated at Burn-In Temperatures," in *Proceedings of IEEE 43rd Electronic Components and Technology Conference* (1993), 88–92, https://doi.org/10.1109/ECTC.1993.346849.

12. F. Almquist, "Button Contacts for Liquid Nitrogen Applications," in *Proceedings., 39th Electronic Components Conference* (1989), 88–91, https://doi.org/10.1109/ECC.1989.77732.

13. K. Xiao, Z. Bai, L. Yan, et al., "Microporous Corrosion Behavior of Gold-Plated Printed Circuit Boards in an Atmospheric Environment With High Salinity," *Journal of Materials Science: Materials in Electronics* 29, no. 11 (2018): 8877–8885, https://doi.org/10.1007/s10854-018-8905-7.

14. J. G. Zhang, "A Summary Report on the Mechanism of Electric Contact Failure Due to Particle Contamination," in *2011 IEEE 57th Holm Conference on Electrical Contacts (Holm)* (2011), 1–8, https://doi.org/10.1109/HOLM.2011.6034803.

15. Z. Wang, J. Gao, Y. Zhou, and Z. Cheng, "High-Frequency Behavior Analysis and Modeling of Silver Plated Printed Circuit Board With Electrochemical Migration," *Journal of Electronic Materials* 48, no. 12 (2019): 8039–8046, https://doi.org/10.1007/s11664-019-07651-3.

16. W. Wang, J. Gao, Z. Wang, T. Zhang, C. Wang, and H. M. Bilal, "Modeling and Analysis of Signal Integrity of High-Frequency Transmission Channel With Degraded Fuzz Button Connectors," *IEEE Transactions on Electromagnetic Compatibility* 66, no. 6 (2024): 1888–1899, https://doi.org/10.1109/TEMC.2024.3422076.

17. X. Gan, H. Qu, X. Mang, C. Wang, and J. Zhu, "Research on ELM Soft Fault Diagnosis of Analog Circuit Based on KSLPP Feature Extraction," *IEEE Access* 7 (2019): 92517–92527, https://doi.org/10.1109/ACCESS.2019.2923242.

18. Z. Wang, J. Li, G. T. Flowers, et al., "Intelligent Detection Methods of Electrical Connection Faults in RF Circuits," *Applied Sciences-Basel* 11, no. 21 (2021): 9973, https://doi.org/10.3390/app11219973.

19. P. G. Slade, *Electrical Contacts: Principles and Applications*. 2nd ed. (CRC Press, 2014).

20. W. Yang, W. Liao, S. Yu, and R. Sun, "Dielectric Properties of Epoxy Nanocomposites Filled With Copper Oxides," in *18th International Conference on Electronic Packaging Technology* (2017), 1212–1215, https://doi.org/10.1109/ICEPT.2017.8046657.